Cuts on Fox-Wolfram Moments

Bachelor Thesis in Physics
submitted by Anja Butter
born in Mayen
SS 2012

This Bachelor Thesis has been carried out by Anja Butter at the
Institute for Theoretical Physics in Heidelberg
under the supervision of
Prof. Dr. Tilman Plehn

Abstract

Fox-Wolfram moments (FWM) are a set of event shape observables that use the total angle between the jets in an event in order to describe the final-state topology of a particular high-energy collision. The properties of this observable will be discussed especially for events with two hard jets. Moreover, the implications of cuts as well as the way they are affected by a special event topology are discussed by means of WBF and a special Drell-Yan process. The goal of this work was to explore the possibility of replacing conventional cuts by cuts on the FWM themselves. Although it was not possible to achieve the same signal to background ratio of 5.9% as conventional cuts by exclusively using FWM cuts, it turned out to be possible to replace simple cuts on the angular distance or the hemisphere and to increase the signal to background ratio from 0.19% to 2.4%.

Zusammenfassung

Als Fox-Wolfram Momente (FWM) bezeichnet man einen Satz Observablen, die die Winkel zwischen den Jets eines Ereignisses nutzen um die Topologie einer bestimmten hochenergetischen Kollision zu untersuchen. Die Eigenschaften dieser Observablen werden insbesondere für Events mit zwei harten Jets diskutiert werden. Darüber hinaus werden die Folgen von Cuts ebenso wie die Auswirkungen spezieller Eventtopologien auf selbige Cuts anhand schwacher bosonischer Fusionsprozesse und eines speziellen Drell-Yan Prozesses diskutiert werden. Ziel dieser Arbeit war es, fest zu stellen, ob konventionelle Cuts durch Cuts an FWM ersetzt werden können. Obwohl es nicht möglich war, allein mit Cuts an FWM das gleiche Verhältnis von Signal zu Hintergrund zu reproduzieren, das mit konventionellen Cuts erreicht wird (5.9%), konnte doch gezeigt werden, dass sowohl einfache Cuts am Winkelabstand als auch der Hemispheren-Cut ersetzt werden konnte. Außerdem konnte das Verhältnis von Signals zu Hintergrundprozess von 0.19% auf 2.4% erhöht werden.

Contents

1 Introduction

The Standard Model (SM) is a theory describing the matter particles and the way they interact with each other. This theory has successfully predicted the results of many different experiments and had its current culmination with the long attended discovery of a new Higgs-like boson this summer [11] [12]. The Higgs boson is the last missing particle in the standard model and makes the theory self-consistent. Nevertheless, there remain unanswered questions. For example, detailed properties of the Higgs boson like its strength of interaction with W- and Z- bosons and also its spin properties. Additionally, although the SM is self consistent, there are other phenomena like dark matter that seem to ask for extensions of the SM.

In order to study the properties of known particles or discover new ones it is crucial to make predictions for experiments and compare them with the real results. For this purpose scientists have devised theoretical event generators which generate computationally the kinematics and frequencies of events for a given theory. After applying event shape observables to the generated as well as the experimental data one can compare the results. In case there are significant differences between the results, the theory is falsified. Else the experiment indicates that the theory is a justified model to describe reality. Another application of event shape observables is the isolation of special processes. Different processes can have different event topologies and so by means of observables that highlight these differences, processes become distinguishable.

This thesis deals with the question of whether it is possible to implement cuts with the help of a special observable - the Fox-Wolfram moments (FWM) - in order to reduce the signal to background ratio for weak boson fusion (WBF).

The second section gives an introduction to theoretical aspects of the work concerning the underlying physics and the investigated processes as well as the used software. WBF and its background process as well as the different characteristics that are useful for their separation are described. In Section 3 the standard kinematic cuts for WBF will be discussed. Section 4 introduces the FWM as an observable and discusses its properties in detail. In the last section we will apply our knowledge from Sections 3 and 4 in order to create new cuts based on the FWM. We will investigate the implications of cuts on FWM and how we can replace classical cuts or create new ones using the event topology for the purpose of achieving a high signal to background ratio.

2 Theoretical Aspects

2.1 Standard Model

The SM orders all so far discovered particles by their spin. Firstly, there are the half-integer spin particles, fermions. The fermions consist of two types of elementary particles: leptons and quarks. These particles can be sorted into three generations that differ by their mass and flavor. Each generation consists of two leptons, namely one electron-like and a neutrino, and two quarks, one with charge +2/3, one with charge -1/3. An overview of these particles can be found in Table 1. Each fermion also has its own antiparticle which leaves us in the end with 12 leptons and 12 quarks.

Second there are the interaction particles, called bosons, with integer spin. There are 12 bosons: the photon for the electromagnetic interaction, $W^{\pm}$ and Z^0 for the weak interaction and eight gluons for the strong interaction. There are also fermions and bosons which are not elementary particles. Due to color confinement quarks never appear as single particles but hadronise. Thereby a quark and an antiquark can form a meson, which is a spin-1 particle, and three (anti-)quarks can build an (anti-)baryon, a fermion.

Finally there is the Higgs particle. The Higgs of the SM is theorized to have spin 0 which means it is a scalar. The Higgs mechanism causes the electroweak symmetry breaking which gives the weak gauge bosons their mass. The insertion of a Higgs field in the Lagrangian for the Standard model also results in a mass term for the fermions. The Higgs particle and the corresponding Higgs-mechanism predicted already in the 1960's [20] [19] could not be detected in the last 50 years. At last on July 4, 2012, the CERN announced a 5 σ evidence for the discovery of a boson that behaves like a Higgs.

2.1.1 Weak Boson Fusion

The Higgs boson can interact with leptons, $W^{\pm}$ and Z bosons, quarks and with itself as illustrated in Fig. 1. The three main production mechanisms for the Higgs are shown in Fig. 2[1]. Sorted by their likelihood, these processes are: gluon fusion,

[1]This graph as well as all other graphs have been created by FeynMF [21].

	electromagnetic charge	1. generation		2. generation		3. generation	
quarks	$+\frac{2}{3}$	u	up	c	charm	t	top
	$-\frac{1}{3}$	d	down	s	strange	b	bottom
lepton	-1	e	electron	μ	muon	τ	tau
neutrino	0	ν_e	electron neutrino	ν_μ	muon neutrino	ν_τ	tau neutrino

Table 1: Fermions of the Standard Model

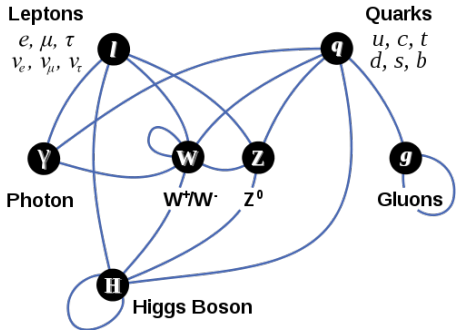

Figure 1: Possible interactions between particles described by the SM. This Figure is taken from [1].

WBF and Higgs strahlung. Although the cross section for gluon fusion exceeds the others by nearly one order of magnitude [22], there are many kinematically similar background processes which make it difficult to isolate this process. Therefore we will look at the WBF that doesn't have such a high cross section but generates a clear signal when one considers the Higgs decay to taus which in turn decay leptonically.

This process generates a Higgs via weak bremsstrahlung. We will reduce ourself to processes with two incoming partons and only allow for $W^{\pm}$ to be emitted and generate a Higgs. A possible process is:

$$ud \rightarrow dd\,W^{+} \rightarrow dd\,W^{+}H \rightarrow du\,H. \tag{1}$$

The up quark emits a W^{+} via weak boson bremsstrahlung. The weak boson emits a Higgs and is absorbed by the second parton. Also we consider gluon initiated processes.

After the WBF there are different decay channels. For a mass of 125 GeV/c^2 the decay channels which have the highest rates are $b\bar{b}$, WW, gg and $\tau\bar{\tau}$. Here the decay into taus generates the cleanest signal when it decays leptonically into electrons or muons. So this is the most probable decay that generates a clear signal while all other decay products would most likely result in additional jets. So the process we will look at is

$$qq \rightarrow H + jj \rightarrow \tau\bar{\tau} + jj. \tag{2}$$

Additionally we will allow the emission of one extra jet during the process. this is done by allowing one hard emission at the matrix element level which is merged

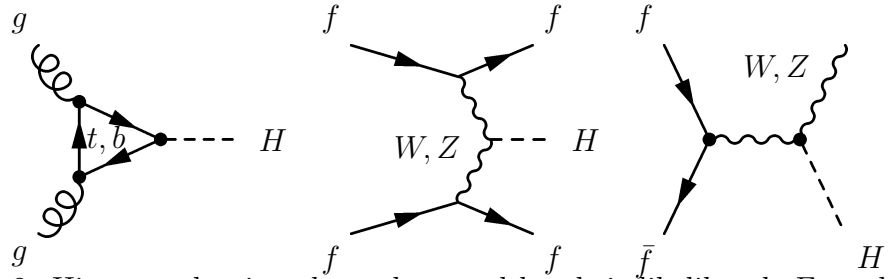

Figure 2: Higgs production channels sorted by their likelihood. From left to right: Gluon fusion, WBF, Higgs strahlung

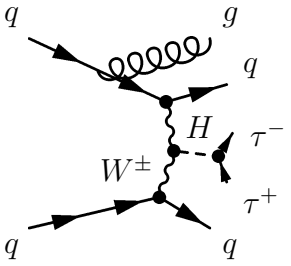

Figure 3: WBF and decay to $\tau\bar{\tau}$

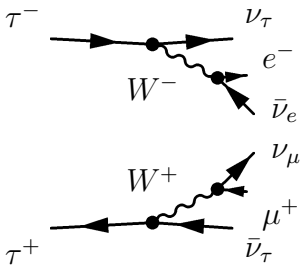

Figure 4: $\tau\bar{\tau}$-decay

with the parton shower using the recent approach of [23]. The entire hard process can be seen in Fig. 3 .

The tau, having a lifetime of $2.9 * 10^{-13}s$ immediately decays into quarks which hadronise (65%) or leptons [14]. A purely leptonic decay of both taus will generate the cleanest signal whereas the most probable process is a decay into an electron and a muon. The Feynman graph for this process is shown in Fig. 4. The probability for a decay into a tau neutrino, an electron and an electron neutrino is 17.83%[14] and for a decay into a tau neutrino, a muon and a muon neutrino 17.41% [14]. This results in a combined probability of 6.20% for the decay of the two taus into an electron and a muon.

Weak boson bremsstrahlung is emitted at small angles. This means that the jets that originate from the remaining partons will generally be forward-backward after the emission. The two taus on the other hand are the decay products of the Higgs. In general, they will tend to be between the two jets. Finally, the extra jet, which can be emitted during the hard process from any of the partons, remains. As we consider the jet to originate from the hard process, this jet can be emitted in any direction.

Summarizing we have two leptons which are central and up to three jets with at least two of them forward-backward and back-to-back. This results in a cross section of 17.1fb including the factor of 6.2% and under the assumption of two protons colliding with 14 TeV.

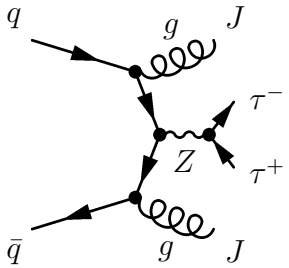

Figure 5: Z+2 Jets decay to $\tau\bar{\tau}$

2.1.2 Background Process

A typical background process for WBF is

$$q\bar{q} \to Z\,jj \to \tau\bar{\tau}\,jj. \tag{3}$$

An example Feynman graph is drawn in Fig. 5. This type of processes is called a Drell-Yan process. Again for the analysis we require that the taus are stable, but in order to compare the cross sections with other results we assume that the taus decay into an electron and a muon similar to the WBF (Fig. 4). Consequently the cross section will also be multiplied by 6.20%.

In this process we allow two extra partons to be emitted during the hard process which are merged to parton showers using the same techniques as for WBF event generation. These jets can be emitted in any direction. Considering all possible processes leads to an overall cross section of 116 pb which we can see overwhelms the signal process cross-section.

2.2 Methods and Software

The first step in order to make any prediction concerning for example WBF is the generation of particles. For this purpose, we use SHERPA [18]. SHERPA is an event generator which calculates the necessary cross sections for a given hard process. Further, SHERPA can merge a hard process containing several emitted partons with the parton shower as well as perform the full hadronisation of the event. This merging technique gives a more realistic description of the event than parton shower alone. After integrating out the cross section SHERPA will shower all remaining particles of the collision which are not declared to be stable (e.g. the taus in the WBF have to be stable for later cuts). Showering means that the high energy particles emitted from the hard process can decay into many lighter particles with less energy. In case of partons these particles can again collide and build more massive hadrons or in the case of leptons they can have a lifetime long enough to be detected by the detector.

For running SHERPA one needs a run card that is composed of different modules. As an example we will regard some extracts of the run card for WBF.

SHERPA uses the Monte Carlo particle numbering scheme [17].

```
(run){
  EVENTS 100000;
  MASS[25]=125.
  MASSIVE[15]=1
  ACTIVE[23]=0
  STABLE[15]=1;
  YUKAWA_B=0.;
  HEPMC2_GENEVENT_OUTPUT=sherpa-event-output0 ;
  EVENT_MODE=HepMC;
  EVT_FILE_PATH=/remote/lin-17a/butter/SHERPA-MC-1.4.0/Examples/LHC_HWW/0;
}(run);
```

The number of events that are generated is set to 100000. The next four lines set properties of particles. The mass of the Higgs is set to 125 GeV. The last lines refer to the output that is made with HepMC2 [13].

```
(model){
```

```
  MODEL=SM;
  CKMORDER=3;
}(model);
```

This part fixes the used model to Standard Model and the order of the Cabibbo–Kobayashi–Maskawa matrix elements that describe the transition amplitude for the decay of one flavoured quark into a different flavoured quark via W boson emission.

```
(processes){
  Process 93 93 -> 25[a] 93 93 93{1}
    Decay   25[a] -> -15 15
  CKKW sqrt(30/E_CMS)
  Integration_Error 0.02 {4,5};
  ME_QED=Off;
  YFS_MODE=0;
  Order_EW 4;
  End process;
}(processes);
```

This module sets the process. In this case there are two initial partons (93) scattering and interacting via W emission to become two partons and a Higgs (25). "93{1}" means that one additional parton is allowed. The next line says that the Higgs has to decay into a tau and an antitau.

```
(beam){
  BEAM_1  2212; BEAM_ENERGY_1 7000;
  BEAM_2  2212; BEAM_ENERGY_2 7000;
}(beam);
```

The last module sets the kinds of particles that are accelerated as well as their energies.

After running SHERPA we now have an event record, generated by HepMC2, with all final state particles and the particles of the hard process.

In the next step the anti-k_T jet clustering algorithm [9] is used for clustering the final state particles (referred to as protojets) to jets. The algorithm makes use of different quantities that will now be explained. Using the spherical coordinate system, the collision is at the origin and the z-axis points along the beam axis. For any kind of object that exits a collision the rapidity y of this object is defined by

$$y = \frac{1}{2} \ln \left(\frac{E + p_z c}{E - p_z c} \right). \tag{4}$$

For massless particles the rapidity simplifies and becomes the pseudo-rapidity

$$\eta = \frac{1}{2} \ln \left(\frac{|\vec{p}| + p_z c}{|\vec{p}| - p_z c} \right) = - \ln \left[\tan \left(\frac{\theta}{2} \right) \right]. \tag{5}$$

This means that the pseudo-rapidity is a measure for the polar angle θ between protojet momentum and beam axis. Jets with a rapidity that approaches infinity (plus or minus) are called forward or backward (respectively). This means that these jets approach the beam line. A rapidity of 0 means that the jets are perpendicular to the beam axis, which can also be called central. Using the rapidity and the azimuthal angle ϕ of each protojet the angular distance between two jets can be defined by

$$R_{ij} = \sqrt{(\Delta y)^2 + (\Delta \phi)^2}. \tag{6}$$

Then we define $d_i = \frac{1}{p_{T,i}}$ for each protojet. Taking all these quantities we can now define a distance d_{ij} between two protojets by

$$d_{ij} = min(d_i, d_j) \cdot \frac{\Delta R_{ij}}{R}. \tag{7}$$

This anti-k_T algorithm calculates d_i for each protojet and d_{ij} between each two protojets. Now the minimum of all d_i and d_{ij} has to be found. If the minimum is a d_{ij}, the corresponding protojets will be combined to a new protojet and the algorithm starts again. If the minimum is a d_i, then the corresponding protojet is promoted to a final jet and will be removed from the list of protojets. Depending on whether there are remaining protojets or not, the algorithm ends or starts again.

The number of jets into which the final state particles are clustered clearly depends on R, which is the only changeable variable. Higher values of R allow wider distances between particles that are clustered into jets. This results in smaller numbers of jets. Typical values for R lie between 0.1 and 1. For this thesis the algorithm is implemented with FastJet [10] setting $R = 0.4$.

Now that the final state particles are clustered to jets, it is necessary to make some cuts. This will be discussed in detail in the next section. After performing the cuts, an observable can be calculated from the jets. These observables characterize for example the distributions of the jet's azimuthal or polar angle. Typical examples are thrust, thrust major, thrust minor and oblateness [6]. In this thesis FWM will be applied. This observable uses the total angle between two jets which distinguishes it from other observables that only take into account the difference in angle between a jet and a fixed axis.

The analysis of the SHERPA results and the subsequent illustrations are done with ROOT [7]. The calculations have been carried out on the bwGRiD[2] and used OpenMP [5] for parallelizing the code.

3 Conventional Cuts

With cuts we can account for the detector conditions and for the relative frequency of signal to background. For example one can not immediately detect the outgoing particles of a hard process. Instead the detector will detect the showered particles. But there are more complications. First of all a jet can not always be assigned to an outgoing particle. The jet forming algorithm can assign two jets to one particle if the decay products are back-to-back or correlate two particles to one jet if there is a broad overlay. Additionally, some particles like neutrinos can not be detected at all while others can only be detected in special solid angles in which the energy resolution depends on the detector. Therefore it is necessary that the generated final state objects fulfill some minimal criteria which take into account the coverage and energy resolution of the detector.

We will account for such problems by implementing cuts on our events so that we only focus on events that are detectable and will generate a clear signal. These cuts also offer another possibility. Using the event topology they enable us to reduce background signals.

3.1 Minimal Cuts

According to the mentioned requirements we have to implement cuts that reduce the high number of events to those which can be detected and will give a clear signal. This means that there have to be at least two jets with a high transverse momentum and a rapidity higher than 5.0. The rapidity cut accounts for the design of the detector. It is not possible to cover the entire polar angle since there must be some space for the beam. Additionally the signal to background ratio gets lower next to the beam line, caused by bremsstrahlung which is mostly emitted at small angles. A cut on the transverse momentum is needed because there is a minimal energy that triggers the detector.

The same is true for the leptons, but due to differences between electromagnetic and hadronic calorimeters we ask for a lower transverse momentum and a smaller rapidity. Let us now define a set of the *initial cuts*:

$$p_{T(lep)} > 10\,\mathrm{GeV} \qquad y_{(lep)} < 2.5 \tag{8}$$

$$p_{T(jet)} > 20\,\mathrm{GeV} \qquad y_{(jet)} < 5.0 \tag{9}$$

By construction through the anti-k_T jet clustering algorithm two jets have to be separated by an angular distance of at least $R = 0.4$. In order to have the two hardest jets (those with highest p_T) well separated, their angular distance has to be at least $R = 0.7$. The same is required for each combination of the two jets with the two leptons. In order to include these two additional cuts let us further define a set of *minimal cuts* composed of the initial cuts and and new ones:

$$\Delta R_{jet,jet} > 0.7 \tag{10}$$

$$\Delta R_{jet,lep} > 0.7 \tag{11}$$

These first cuts leave us with two detectable and well separated jets and leptons. We have to implement further cuts to reduce the background.

3.2 Weak Boson Fusion Cuts

While the minimal cuts were geared to conditions imposed by the detector and the jet clustering algorithm, the following cuts use the properties of the signal process to increase the signal to background ratio. Recalling the event topology for WBF we have two jets that are forward-backward and two central leptons that are back-to-back. Zjj on the other hand has two jets that are emitted in an arbitrary direction. This leads us to the following cuts:

$$y_{j_{min}} + 0.7 < y_{lep} < y_{j_{max}} - 0.7 \tag{12}$$

Obviously this cut results in $\Delta R_{jet,jet} > 1.4$ and $\Delta R_{jet,lep} > 0.7$ and so implies the preceding cuts.

With the next cut we want to separate the tagging jets in the different hemispheres. Therefore we demand:

$$y_1 * y_2 < 0 \tag{13}$$

Combining this cut with the previous one results in a minimal angle difference of $\Delta\theta = 27.4°$ for the massless case.

Additionally, we require that the two hardest jets are relatively forward-backward. This is achieved by

$$|y_{j_1} - y_{j_2}| > 4.4. \tag{14}$$

This cut also implies equation (10). Respecting the minimal cuts, in the massless case, this corresponds to a minimal angle of 56.7° between the hardest jets. Taking into account equation (13), this cut even requires a minimal angle of 88.39° and one jet with $\theta < 12.65°$ with respect to the beam axis .

Observations have shown that in general for QCD processes the two hardest jets have a smaller invariant mass than for EW processes [22]. Therefore the last cut demands a minimal invariant mass $M_{ij} = \sqrt{(E_i + E_j)^2 - (\vec{p_i} + \vec{p_j})^2}$ of the two hardest jets.

$$M_{ij} > 600\,\text{GeV} \tag{15}$$

3.3 Cutflow

Table 2 and 3 show the evolution of the cross section for both processes and the signal to background ratio. The cross sections are calculated for the hard process including the decay of the taus into electron and muon. Applying all cuts, the signal to background ratio increases from 0.0148% to 5.9%. For each cut there is also the percentage of events that are removed and the enhancement which is defined by

$$\text{Enhancement} = \frac{\%\text{ signal surviving cut}}{\%\text{ background surviving cut}}. \tag{16}$$

Cut	HWW		QCD Zjj		Signal / Background	
	Cutoff[%]	cs [fb]	Cutoff[%]	cs [fb]	Enh.	S/B[%]
Hard process		17.2		116000		0.0148
$p_{T(lep)} > 10\,\text{GeV}$	2.9	16.7	6.1	109000	1.03	0.0153
$y_{(lep)} < 2.5$	23.3	12.8	47.7	57100	1.46	0.022
$p_{T(jet)} > 20\,\text{GeV}$ & $y_{(jet)} < 5.0$	31.2	8.81	91.9	4640	8.8	0.19
total	0.49		0.96		12.8	

Table 2: Cutflow of signal and background process for the initial cuts. The cross section are calculated including the additional factor for the decay of two taus into an electron and a muon.

Cut	HWW		QCD Zjj		Signal / Background	
	Cutoff[%]	cs [fb]	Cutoff[%]	cs [fb]	Enh.	S/B[%]
after initial cuts		8.8		4640		0.19
$\Delta R_{jet,jet} > 0.7$	3.2	8.5	4.5	4430	1.01	0.19
$\Delta R_{jet,lep} > 0.7$	8.2	7.8	15.0	3770	1.08	0.21
$y_{j_{min}} + 0.7 < y_{lep}$ & $y_{lep} < y_{j_{max}} - 0.7$	50.6	3.9	92.3	289	6.5	1.3
$y_1 * y_2 < 0$	3.9	3.7	13.8	249	1.1	1.5
$\lvert y_{j_1} - y_{j_2} \rvert > 4.4$	26.9	2.7	63.9	90.0	2.0	3.0
$M_{ij} > 600\,\text{GeV}$	19.1	2.2	58.7	37.2	2.0	5.9
total	75.0		99.2		31.2	

Table 3: Cutflow of signal and background process after the initial cuts. The cuts are applied sequentially.

We find that for the initial cuts the signal to background ratio is strongly increased by the first cut on the jets which reduces the background by 91.9%. This is the reason why we call these cuts initial cuts. The first two cuts can already be applied before the jet clustering algorithm and the third cut also has to be applied before any further analysis as it reduces the number of background processes by more than one order of magnitude. From here on we will only work with events that have fulfilled these initial cuts.

Looking at the cuts of Table 3, the cut which orders jets and leptons in space clearly has the highest enhancement followed by Δy and M_{ij}. The enhancement and the cutoff for a particular cut also depend on the order in which the cuts are performed. Table 4 shows the enhancement for each cut alone applied after the initial cuts. Here we see that especially for 2-jet events the enhancement of the cut on the invariant mass is higher than both other cuts.

Cut	all events WBF	QCD Zjj	Enh.	2 jet events WBF	QCD Zjj	Enh.
$\Delta R_{jet,jet} > 0.7$	3.2	4.5	1.01	2.2	4.8	1.03
$\Delta R_{jet,lep} > 0.7$	8.0	14.5	1.08	7.6	14.7	1.08
$y_{j_{min}} + 0.7 < y_{lep}$ & $y_{lep} < y_{j_{max}} - 0.7$	56.1	93.8	7.0	52.5	93.7	7.5
$y_1 * y_2 < 0$	31.0	60.0	1.7	27.3	60.6	1.8
$\lvert y_{j_1} - y_{j_2} \rvert > 4.4$	63.0	95.7	8.5	59.4	95.4	8.9
$M_{ij} > 600\,\text{GeV}$	66.4	97.1	11.7	64.2	98.1	19.2

Table 4: Properties of each cut applied immediately after the initial cuts.

4 Fox-Wolfram Moments

The FWM are an event shape observable that depends on the momenta of the jets as well as the total angle between each two jets. This dependency distinguishes it from other observables that only take into account the difference in angle between a jet and a fixed axis.

4.1 General Properties of the Fox-Wolfram Moments

4.1.1 Definition

Originally [16] the FWM are defined by:

$$H_l = \frac{4\pi}{2l+1} \sum_{m=l}^{-l} \left| \sum_i Y_l^m(\theta_i, \phi_i) \frac{|\vec{p_i}|}{\sqrt{s}} \right|^2 . \tag{17}$$

where Y_l^m denotes the spherical harmonics and θ and ϕ the usual spherical coordinates.

This definition can be converted into the form:

$$H_l = \frac{4\pi}{2l+1} \sum_{m=l}^{-l} \left(\sum_i Y_{lm}(\theta_i, \phi_i) \frac{|\vec{p_i}|}{\sqrt{s}} \right) \left(\sum_j Y_{lm}^*(\theta_j, \phi_j) \frac{|\vec{p_j}|}{\sqrt{s}} \right) \tag{18}$$

$$= \sum_{i,j} \frac{|\vec{p_i}|\,|\vec{p_j}|}{s} \frac{4\pi}{2l+1} \sum_{m=l}^{-l} Y_{lm}(\theta_i, \phi_i) Y_{lm}^*(\theta_j, \phi_j) \tag{19}$$

$$= \sum_{i,j} \frac{|\vec{p_i}|\,|\vec{p_j}|}{s} P_l(\cos\Omega_{ij}). \tag{20}$$

The last equality uses the addition theorem for spherical harmonics. This form now shows that the FWM depend on the total angle Ω between the jets. They are computed as the sum over all possible combinations of jets, including the combination of a jet with itself. In general the Legendre polynomials are weighted with some factors W_i and W_j:

$$H_l = \sum_{i,j} \frac{W_i W_j}{s} P_l(\cos \Omega_{ij}). \tag{21}$$

We will see how the shape of the event shape observables depends on the choice of weight and normalization factors.

Before applying the FWM to our processes we take a look at the general properties of the FWM:

Originally the FWM have been defined by $W_i = |\vec{p_i}|$ and $\sqrt{s} = \sum_i |\vec{p_i}|$ [16]. In some cases it will turn out to be more promising to use the transverse momenta $p_{T,i}$ as weight and normalization factor like suggested in [15] but for the moment it is more illustrating to work with the original definition. As the general properties do not differ in the choice of $|\vec{p_i}|$ vs. $p_{T,i}$ we will postpone the discussion of these differences to a later section.

4.1.2 Dependence on Angles $\Delta\phi$ and $\Delta\theta$

Up to now we only treated the FWM as an observable that depends on $\Omega_{i,j}$. Instead we can also separate the angle in ϕ and θ components. When we express the jets in spherical coordinates we can write:

$$\vec{p_i} = |\vec{p_i}| \begin{pmatrix} \sin\theta_i \cos\phi_i \\ \sin\theta_i \sin\phi_i \\ \cos\theta_i \end{pmatrix} \tag{22}$$

Now the angle between two jets can be expressed by

$$\cos \Omega_{i,j} = \frac{\vec{p_i}\vec{p_j}}{|\vec{p_i}| \cdot |\vec{p_j}|} \tag{23}$$

$$= \sin\theta_i \sin\theta_j (\cos\phi_i \cos\phi_j + \sin\phi_i \sin\phi_j) + \cos\theta_i \cos\theta_j \tag{24}$$

$$= \frac{1}{2}(\cos\Delta\theta - \cos\square\theta)\cos\Delta\phi + \frac{1}{2}(\cos\Delta\theta + \cos\square\theta), \tag{25}$$

where $\Delta\theta = \theta_i - \theta_j$ and $\square\theta = \theta_i + \theta_j$. The last equality uses the addition theorems. Looking at equation (25) we see that the dependence of $\cos\Omega_{ij}$ and therefore H_l on ϕ becomes maximal if both jets are perpendicular to the beam axis so that $\cos\Delta\theta = 1 = -\cos\square\theta$ and minimal if there is no difference between $\cos\Delta\theta$ and $\cos\square\theta$. This difference goes to zero if one of the jets is parallel to the beam line ($\theta_i \to 0/\pi$ respectively). Considering the event topology of the WBF, one can assume that both jets are close to the beam axis. In this case the cosines ($\cos\Omega_{i,j}$, ...) can be expressed by:

$$\cos\Delta\theta \approx -1 + \frac{(\pi - \theta_1 + \theta_2)^2}{2} \tag{26}$$

$$\cos\square\theta \approx -1 + \frac{(-(\pi - \theta_1) + \theta_2)^2}{2} \tag{27}$$

$$\cos\Omega_{i,j} \approx -1 + (\pi - \theta_1)\theta_2 \cos\Delta\phi + \frac{1}{2}((\pi - \theta_1)^2 + \theta_2^2) \tag{28}$$

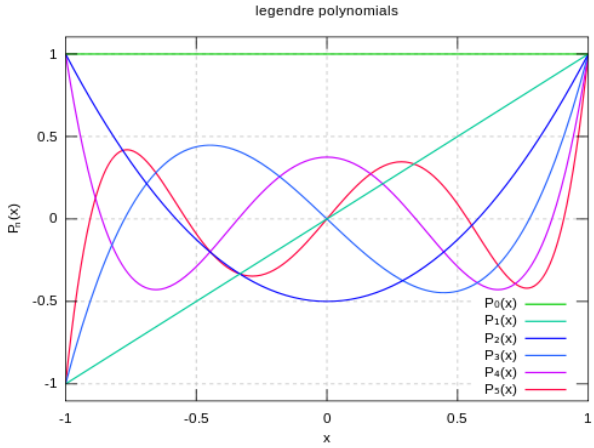

Figure 6: Legendre Polynomials in the range $-1 \leq x \leq 1$ for $l = 0, \ldots, 5$. Figure taken from [3]

4.1.3 Legendre Polynomials

If we want to understand the FWM defined by

$$H_l = \sum_{i,j} \frac{|\vec{p_i}|\,|\vec{p_j}|}{(\sum_i |\vec{p_i}|)^2} P_l(\cos\Omega_{ij}) \tag{29}$$

we first have to take a look at the Legendre Polynomials.

As $-1 \leq \cos\Omega_{ij} \leq 1$ it is helpful to visualize the Legendre polynomials in this range (s. Fig. 6). The following observations are generally valid and can be verified under [4]. The Legendre polynomials P_l are polynomial functions of degree l. We can see that $P_l(1) = 1$ (equating $\Omega_{ij} = 0$) for all l. As the Legendre polynomials with even l are even functions, $P_l(x) = P_l(-x)$. This means that $P_l(-1) = P_l(1) = 1$, giving jets that are back-to-back the same weight factor as jets which go nearly in the same direction. In turn the Legendre polynomials become odd functions for odd values of l, $P_l(x) = -P_l(-x)$. This includes for example that $P_l(0) = -P_l(-0) = 0$ ($\Omega_{ij} = \pi/2$). As a consequence, combinations of jets that are perpendicular to each other do not contribute. Additionally, for all l it is $-1 \leq P_l(x) \leq 1$ with $-1 \leq x \leq 1$. In general the range of H_l for all values of P_l is

$$\frac{\sum_j |\vec{p_j}|^2}{(\sum_k |\vec{p_k}|)^2} - 2\frac{\sum_{i<j} |\vec{p_i}|\,|\vec{p_j}|}{(\sum_k |\vec{p_k}|)^2} \leq H_l \leq \frac{\sum_{i,j} |\vec{p_i}|\,|\vec{p_j}|}{(\sum_k |\vec{p_k}|)^2} = 1. \tag{30}$$

For a more detailed investigation we have to take a closer look at the precise form of the FWM.

The equations for the first Legendre polynomials are explicitly written down in Table 5. Using P_0 and P_1 one can use Bonnet's recursion formula

$$(l+1)P_{l+1}(x) = (2l+1)xP_l(x) - lP_{l-1}(x) \tag{31}$$

to compute higher orders of P_l.

	Legendre Polynom	extremum (x_0)	$P_l(x_0)$	min/max
$P_0(x)$	1			
$P_1(x)$	x			
$P_2(x)$	$(3x^2-1)/2$	x=0	-0.5	min
$P_3(x)$	$(5x^3-3x)/2$	x=$\pm\frac{1}{\sqrt{5}}=\pm 0.447$	∓ 0.447	min/max
$P_4(x)$	$\frac{1}{8}(35x^4-30x^2+3)$	x=0	0.375	max
		x= $\pm$ 0.65	-0.43	min
$P_5(x)$	$\frac{1}{8}(63x^5-70x^3+15x)$	x= $\pm$ 0.77	∓ 0.42	min/max
		x= $\pm$ 0.29	± 0.35	max/min

Table 5: Legendre Polynomials with their corresponding extrema

4.1.4 Special Cases

Now we take a look at the first two FWM. Setting $l = 0$:

$$H_0 = \sum_{i,j} \frac{|\vec{p_i}|\,|\vec{p_j}|}{(\sum_k |\vec{p_k}|)^2} = \frac{\sum_i |\vec{p_i}| \sum_j |\vec{p_j}|}{(\sum_k |\vec{p_k}|)^2} = 1. \tag{32}$$

This may not seem interesting as it leads to the same result for each event but this result is up to the the choice of the normalization factors. If one would choose the energy of the colliding partons for the denominator and the energy of the emitted jets in the numerator, the result could tell us something about energy conservation.

Now we set $l = 1$. In this case it is:

$$H_1 = \sum_{i,j} \frac{|\vec{p_i}|\,|\vec{p_j}| \cdot \cos\Omega_{ij}}{(\sum_k |\vec{p_k}|)^2} = \frac{\sum_{i,j} \vec{p_i}\vec{p_j}}{(\sum_k |\vec{p_k}|)^2} = \frac{(\sum_i \vec{p_i})^2}{(\sum_k |\vec{p_k}|)^2}. \tag{33}$$

As the numerator and denominator are quadratic, H_1 is positive definite. It can approach one as a maximum only if all jets would join the same direction. Considering the event topology of the WBF we do not expect many results for H_1 that are near one after the cuts. On the contrary, H_1 depends on the sum over the momenta of all outgoing jets that are considered in the calculation. As soon as the center of mass of these jets (the center of mass system (CMS) built by these jets) does not move with respect to the chosen coordinate system the result will be $H_1 = 0$. Since we consider the hardest jets, we can anticipate that the CMS only moves slightly and will result in $H_1 \approx 0$. For higher orders of H_l it becomes difficult to analyse them for an arbitrary number of jets. Therefore we discuss the higher orders in the next section where we have reduced the number of jets.

4.2 2-Jet Events

About 80% of the WBF events surviving the initial cuts only have two hard jets. This makes it reasonable to consider the explicit analytical form of the FWM for

2-jet events. Additionally the form of events with more than two hard jets is also strongly influenced by the two hardest jets as their momenta are used as weight factors. The consideration of 2-jet events builds a basis for further analysis. A detailed consideration of events with three or more jets can be found under [8].

4.2.1 Special Properties

If we assume there are two jets with $|\vec{p_2}| = r \cdot |\vec{p_1}|$ with $0 \leq r \leq 1$ ($|\vec{p_2}| \leq |\vec{p_1}|$) we can expand the sum explicitly to get:

$$H_l = \frac{|\vec{p_1}|\,|\vec{p_1}|\,P_l(\cos\Omega_{1,1}) + 2\,|\vec{p_1}|\,|\vec{p_2}|\,P_l(\cos\Omega_{1,2}) + |\vec{p_2}|\,|\vec{p_2}|\,P_l(\cos\Omega_{2,2})}{(\sum_{k=1}^{2}|\vec{p_k}|)^2} \tag{34}$$

$$= \frac{P_l(\cos 0) + 2rP_l(\cos\Omega_{1,2}) + r^2 \cdot P_l(\cos 0)}{1 + 2r + r^2} \tag{35}$$

$$= \frac{1 + 2rP_l(\cos\Omega_{1,2}) + r^2}{1 + 2r + r^2} \tag{36}$$

In this case it is easy to see that $H_l > 0$ as the minimal value P_l can assume is -1. Then the denominator can be written as $(1-r)^2$ which has to be positive.

We can further simplify this relation by assuming that the two jets build a CMS. In this case it is $r = 1$ and $\cos\Omega_{1,2} = -1$ which leads to $P_{2l}(\cos\Omega_{1,2}) = 1$ and $P_{2l+1}(\cos\Omega_{1,2}) = -1$. This implies that $H_{2l} = 1$ and $H_{2l+1} = 0$.

However in general - even if we have a 2-jet event - we neglect weak jets so that the two hardest jets do not build a CMS system. Hence the two jets can differ in the absolute value of the momentum ($r \neq 1$) as well as not being exactly back-to-back ($\cos\Omega_{1,2} \neq -1$). Nevertheless, the tendency is still there as one can see in Fig. 8.

In this case we can still visualize the FWM depending on two parameters (r and Ω) for different values of l as it has been done in Fig. 7.

As we can see the FWM only depend weakly on the angle if r approaches 0. In this case they become independent of l. For $r \to 1$ one can clearly see the shape of the Legendre Polynomial. This implies that for increasing l the FWM become very sensitive to the angle between the jets. Next, we apply them to our processes.

4.2.2 Application of the Fox-Wolfram Moments

Let us now investigate explicitly the difference in shape between odd and even FWM up to $l = 1, \ldots, 4$. The FWM are calculated after the initial cuts as further cuts affect the properties of the surviving events such that some details are no longer visible. This will be discussed further in section 4.2.5 see Fig. 13.

The graphics in Figure 7 show that for odd l there are in general three regions.

1. The red regions with high FWM for small ratios $r < 0.3$ or small angles $\Omega < 20°$
2. The yellow and green regions with intermediate FWM
3. The blue regions with small FWM down to 0 for large angles $\Omega > 160°$

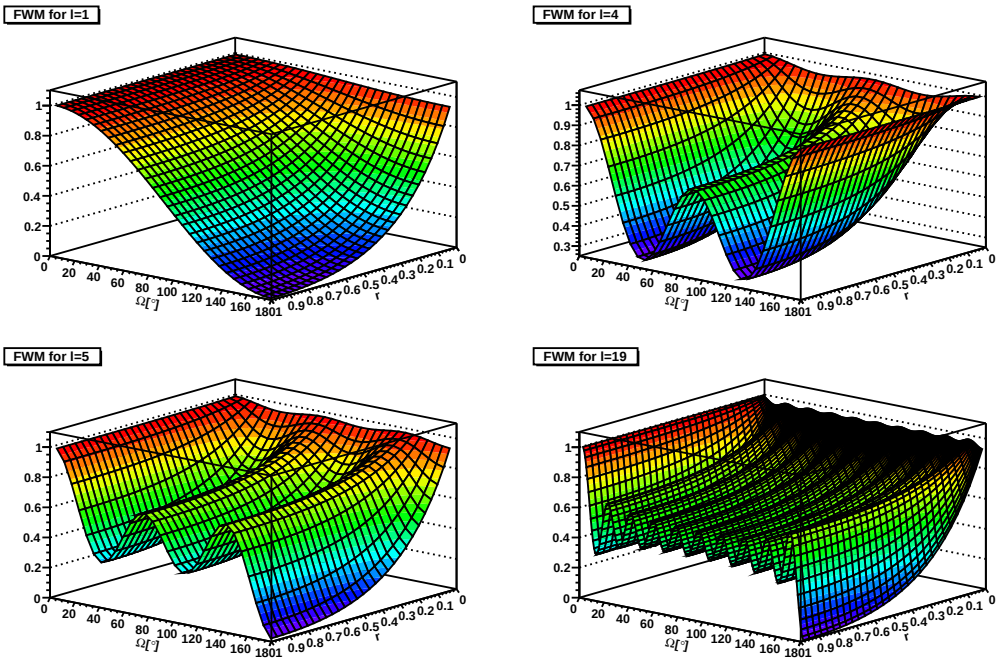

Figure 7: Theoretical shape of the FWM for two jets

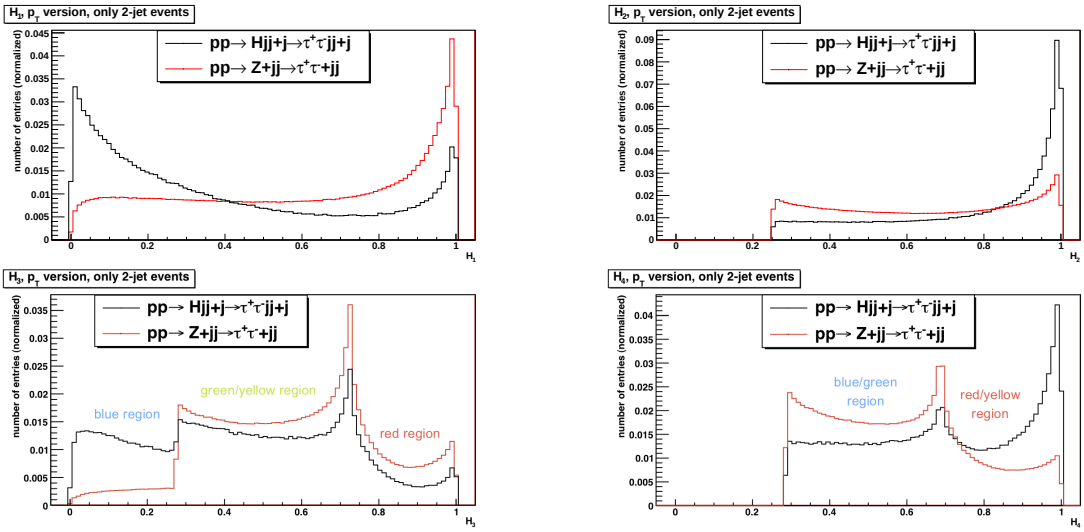

Figure 8: Distribution of the FWM for WBF and Zjj events as weighted with p_T.

Actually we really can identify these regions when we look at Figure 8 for $l = 3$. The blue region is located between 0 and the first peak, the green and yellow is between the first and the second peak and the red region begins after the second peak and goes until $H_3 = 1$.

For even l the FWM are symmetric around 90° and do not go down to 0. Here we only have two regions.

1. The red and yellow regions with high FWM for small ratios $r < 0.2$ or angles

approaching 0° or 180° ($\Omega < 20°$,$\Omega > 160°$)

2. The blue and green regions with FWM between 0.3 and 0.7 for large angles $\Omega > 160°$

Fig. 8 again nicely illustrates this behavior for $l = 4$. For $l = 2$ and $l = 4$ we can see that WBF strongly peaks at $H_l = 1$, which was expected for even l. However for Zjj this is not the case, which indicates the different event topology.

We will use H_5 as an example to illustrate our more detailed observations in Fig. 9.

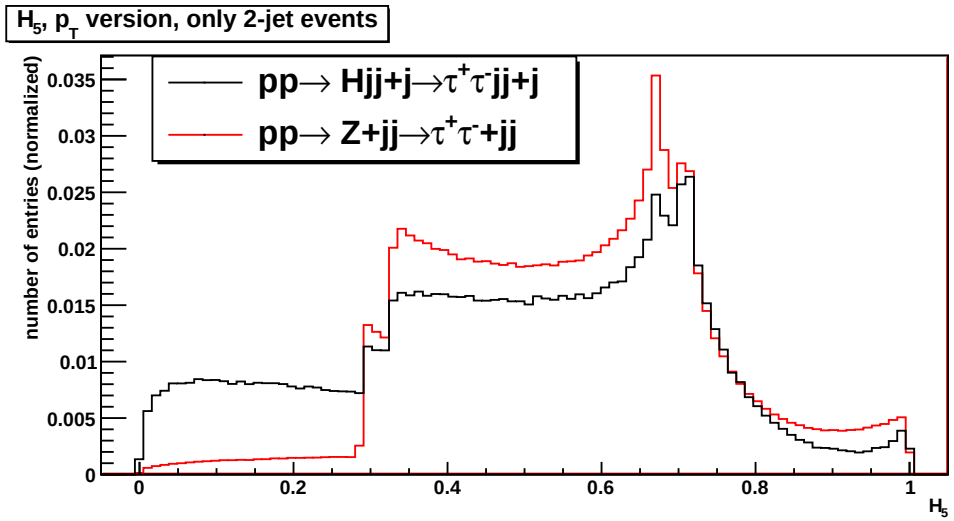

Figure 9: FWM for $l = 5$. We can see two cuts around $H_5 = 0.3$ and two peaks around $H_5 = 0.7$

Here, we can also observe some additional features of the 2-jet events. Around 0.29 and 0.33 there seem to be two cuts and we can see two peaks at 0.67 and 0.72. These cuts and peaks result from the shape of the Legendre polynomial. Considering P_5 we know that its lowest minima lies at $P_5(0.77) = -0.42$. For $r = 1$ the corresponding FWM is $H_5 = 0.29$. This is exactly the same value at which we can see the first cut. The same is true for the other cut and peaks. The cut at 0.33 corresponds to the minimum $P_5(-0.29) = -0.35$ whereas the peak at 0.67 corresponds to the maximum at $P_5(0.29) = 0.35$ and the peak at 0.72 to $P_5(-0.77) = 0.42$.

But how exactly do the cutoffs arise? Looking back again at the different regions we see that the lowest FWM originate from angles above 165° and $r > 0.3$. But as soon as we enter the region of $H_5 \geq 0.29$ suddenly a broad range around 40° where the FWM only weakly depend on r for $1 > r > 0.5$ enters into the distribution. Thus the number of events makes its first step. The same happens again when the range around 108° is added to the distribution. In principle the same also happens at the peaks despite the fact that for small r all events result in high FWM - independent of angle. The peaks originate from the sudden broad region in angle for events which result in the same FWM.

4.2.3 $|\vec{p}|$ versus p_T

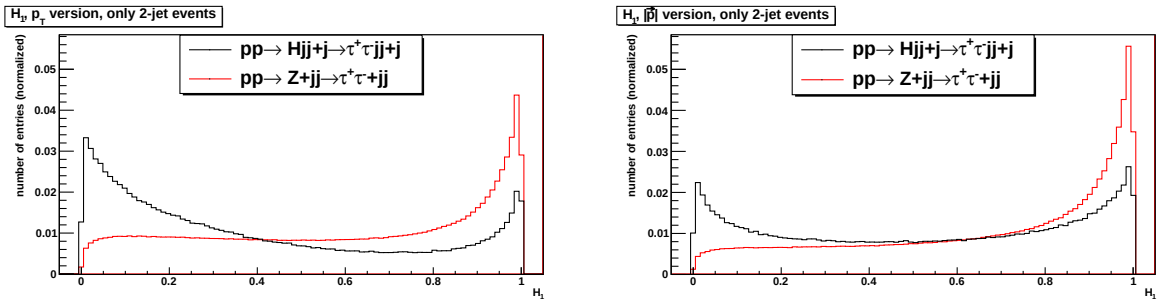

Figure 10: H_1 for WBF and Zjj for 2-jet events. On the left the weight factor is p_T on the left it is $|\vec{p}|$

Now that we know how the applied FWM look we just take a short glance at the choice of the weight factor. Figure 10 shows H_1 for WBF and Zjj one time for $|\vec{p}|$ and one time for p_T as weight factors. One can clearly see that for p_T the processes are easier to distinguish, which is also true for all other values of l. But why is this so? We already know that for $r \to 1$ the FWM become more sensitive to the angle between the jets. The transverse momentum of jets is often small compared to their total momentum as they are more likely to be emitted from partons at small angles. At the same time, the initial cuts require a minimal p_T of 20 GeV. As a consequence many jets have a transversal momentum between 20 GeV and 60 GeV, which automatically results in higher values of r compared to the weight factor $|\vec{p}|$. This distribution of the processes in r and Ω is also shown in Fig. 11. We will use p_T because the FWM are more sensitive to the angles and consequently the processes are easier to distinguish.

4.2.4 Comparing the Two Processes

In section 4.2.2 we applied the FWM (weight factor p_T) to the two processes and found some differences. For example, Zjj peaks at $H_1 = 1$ instead of $H_1 = 0$ and for H_2 Zjj nearly has a flat distribution. For H_3 there are also significantly less events in the range of small momenta while again there is only a small peak at $H_4 = 1$. In order to find out where these differences come from, we compare the r-Ω-distribution from WBF with Zjj for 2-jet events in Fig. 11.

We can see that for WBF the maximum of the distribution lies around 174° while for Zjj it is around 30°. Considering H_1 this results in FWM smaller than 0.2 for WBF and bigger than 0.8 for Zjj. Due to the same reason we do not find many jets in the region with small Fox-Wolframs moments for H_3.

We can also observe that the Zjj distribution is very broad while the WBF peaks sharply. This peak can be used to illustrate another effect: When we go to high FWM we can scan through the angular distribution.

As explained before the peaks which we can observe result from the shape of the Legendre polynomials and their dependence on the angle. If we now look at H_{19} in

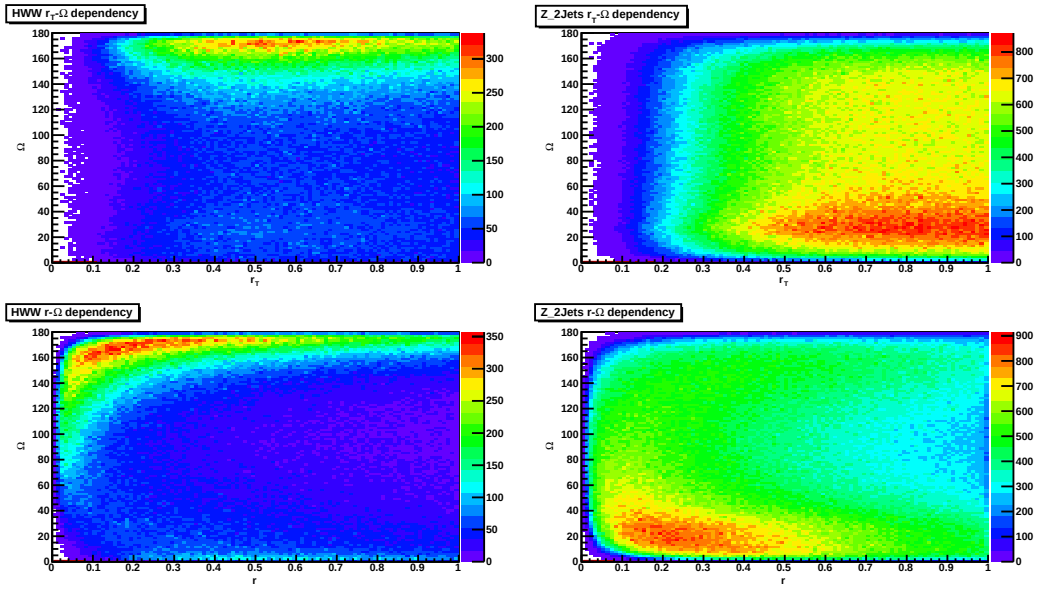

Figure 11: r-Ω-distributions for 2-jet events after the initial cuts. The graphs show differences between WBF and Zjj (left/right) and p_T and $|\vec{p}|$ (top/bottom)

Fig. 12 for the slice $r = 1$ the maxima of the wiggles are all around $H_{19} = 0.6$. This results in the broad peak in Figure 12. Only the maximum at 170° corresponds to a higher FWM: $H_{19} = 0.7$. Because of the high density of the $r - \Omega-$distribution of WBF in this region we can see a sharp peak in Figure 12, while the graph remains smooth for Zjj. We can state that in general for increasing and odd values of l the highest local maximum becomes sharper and moves through the range in angle where now most of the 2-jet events are located. This scanning effect starts for $l = 11$ and will vanish again for high values of l when the last wiggle has passed 175°.

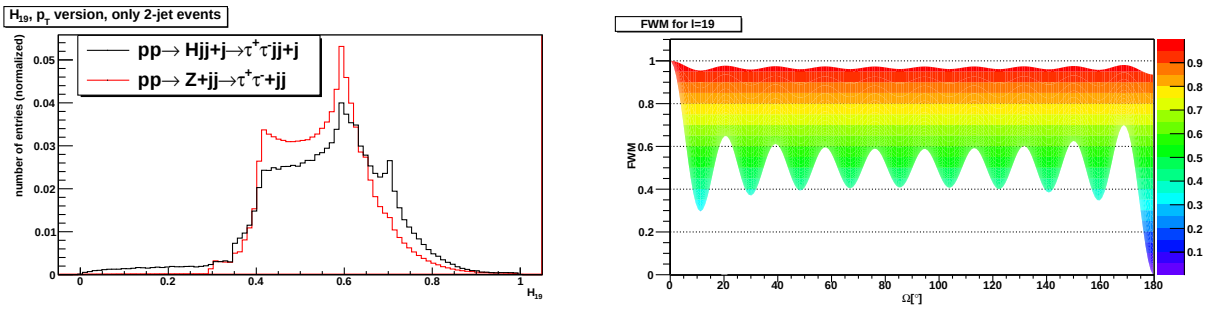

Figure 12: H_{19} for 2-jet events. Left: Applied on WBF and Zjj. Right: Front view on the theoretical shape depending on Ω. The color corresponds to the FWM that are possible for this angle

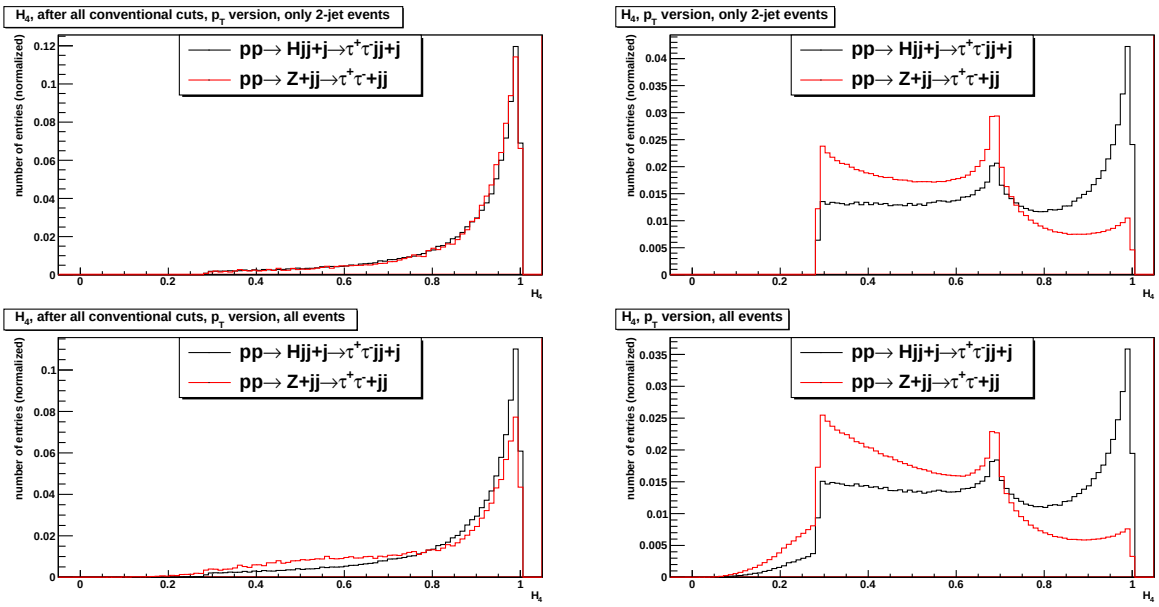

Figure 13: H_4 for 2-jet and n-jet events after (left) and before (right) the cuts

4.2.5 Events With More Than Two Hard Jets

Now that we have investigated 2-jet events we want to see whether there are differences between their FWM and the FWM for events with an arbitrary number of jets. Fig. 13 shows H_4 for 2-jet and n-jet events. In general the distributions are rather similar. The main difference is that there are now FWM smaller than 0.29. This is because a third jet can decrease the numerator if the angles between the third jet and the hardest jets results in a negative value of the Legendre Polynomial.

Fig. 13 also shows the distribution for 2-jet and n-jet events after all the cuts. After the cuts there is nearly no difference between the two processes for 2-jet events because the cuts only allow special configurations of the two hardest jets. That is, that they can only have a special angle with respect to each other which therefore erases all differences in the event topology. However, for the events with more than 2 jets we can still see a difference after the cuts, because the third (fourth, ...) jet is allowed to have an arbitrary angle with respect to the first two jets as long as it has a $p_T > 20\,\text{GeV}$ and $\eta < 5.0$. So here we can see yet more of the properties of the event. The fact that the cuts result in similar shaped FWM suggests that it is also possible to go the other way round. So we will try to imitate the conventional cuts by cutting on the FWM.

5 Cutting on the Fox-Wolfram Moments

After investigating the cuts that are applied to the signal and background processes as well as the properties of the FWM, we can combine this knowledge in order to replace ordinary cuts by FWM cuts. Since cuts on the FWM can only replace cuts that use properties of the jets, the initial lepton cuts have to be kept. Additionally we will keep the initial cuts for the jets which requires two jets with a minimal transverse momentum p_T and a maximal rapidity $|y|$. On the one hand this cut guarantees a good energy resolution and a detectable angle. In the following, the above mentioned cuts will be referred to as the initial cuts.

In order to replace cuts, it is necessary to work with all events. Therefore we will no longer restrict the calculation of the moments to 2-jet events. At the same time it will be possible to explain many effects using as an example the 2-jet events since after the initial cuts the percentage of 2-jet events is 77.8% for WBF and 70.8% for Zjj. Essentially, the effect of additional jets that are weaker than the two hardest jets can be seen as corrections to the result for the two hardest jets.

5.1 Replacing Conventional Cuts by Fox-Wolfram Moment Cuts

After the initial cuts are made, we take a look at how the FWM of the events change with the addition of each cut in sequence. WBF will be considered first. In Fig. 14 and 15 we can see how the FWM change with cuts for different value of l. The total number of events entering the analysis is normalized to one, as can be seen for example for $l = 0$. So the highest line (black line) corresponds to all events entering the analysis and the underlying lines to the events that remain after a cut.

Looking at the development of the FWM for $l = 1$, we see it is convenient to make an acceptance cut for $H_1 < 0.75$. In order to control that we don't remove many events that would not have been removed by the conventional cuts, we calculate the percentage

$$P = \frac{N_{FWM+CC}}{N_{CC}} \cdot 100 \tag{37}$$

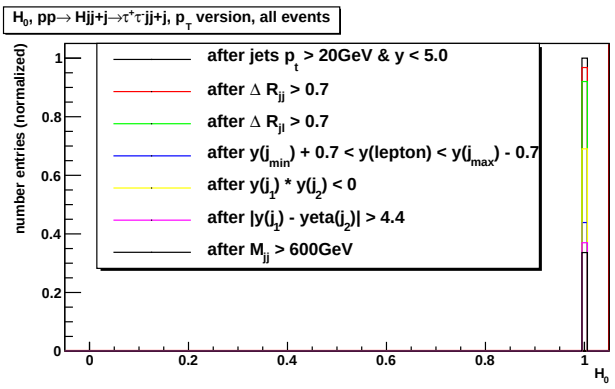

Figure 14: Cutflow of the FWM for WBF for $l = 0$ weighted with p_T, initial cuts performed, with n-jets.

whereas N_{CC} denotes the number of events surviving all conventional cuts and N_{FWM+CC} denotes the number of events passing all conventional cuts and the additional FWM cut. N_{CC} corresponds to the integrals under each lowermost line in Fig. 14 and 15. For the acceptance cut $H_1 < 0.7$ it is P=99.8%. As we do not want to cut more than necessary to replace the cut, we want to keep this ratio close to 1. Let us now see how well the cuts have been replaced. As expected, the number of events that are removed by the original cuts after applying the FWM cut is significantly reduced. In order to quantify by how well a cut can be replaced by a FWM cut we calculate the replacement *rep* by the following equation:

$$rep = \frac{N_{FWM} - N_{FWM+CC_i}}{N_{INIT} - N_{CC_i}} \cdot 100 \tag{38}$$

In the denominator we find the number of events that are removed by each cut CC_i after the initial cuts are applied. It is calculated by subtracting the number of events that survive a special cut N_{CC_i} from the number of events that pass the initial cuts N_{INIT}. Notice that here the cuts will not be applied one after another but each immediately after the initial cuts. In the numerator the number of events that are removed by a special cut after the application of the FWM cut is calculated. N_{FWM} indicates the number of events passing the FWM cut after the initial cut and N_{FWM+CC_i} identifies again the number of events that survive all conventional cuts in addition to the FWM cut. Calculating this fraction results in a ratio between 0 and 1 for each cut. 1 minus the result tells us by which percentage the cut can be replaced. If the cut can be replaced completely the percentage will go up to 100% - which is our goal.

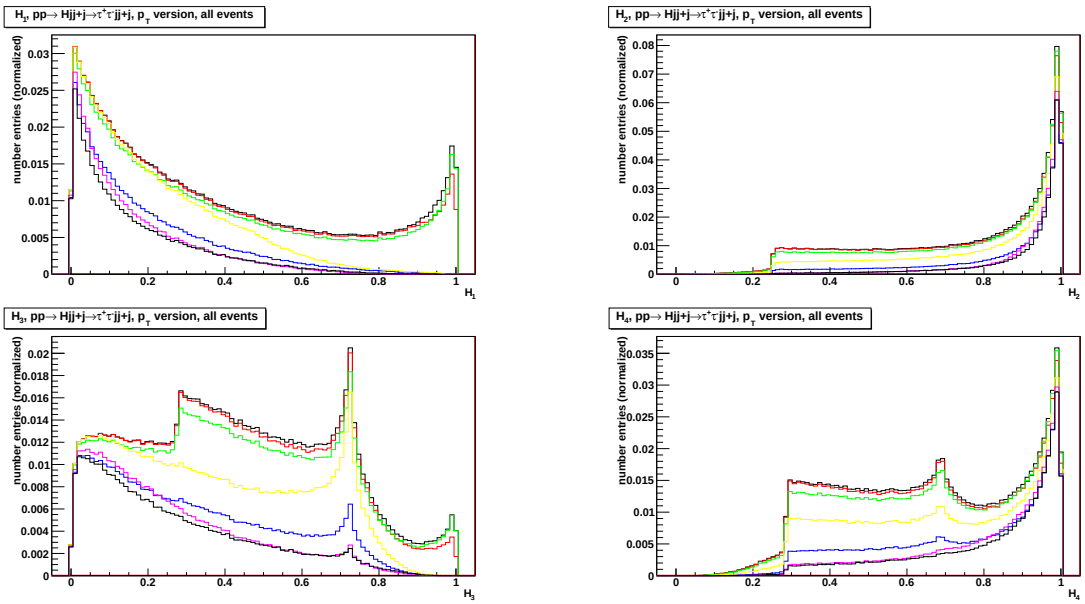

Figure 15: Cutflow of the FWM for WBF for $l = 1, \ldots, 4$ weighted with p_T, initial cuts performed, with n-jets.

Performing this procedure for H_1, we find that the percentage of events removed by the FWM is 68.6% for the $\Delta R_{jet,jet}$-cut and 56.4% for the hemisphere cut.

The described analysis has been done for different FWM for the signal and background processes. The results of this investigation are shown in Table 6 and 7.

The statistics can tell us which conventional cuts can be replaced. Requiring $H_1 < 0.65$ keeps 99.1% of the events after the conventional cuts are applied for WBF and 99.4% for Zjj but cuts 68.5% and 66.4% (respectively) of the events that would be remove by $y_1 * y_2 < 0$. For the first conventional cut $\Delta R_{jet,jet} > 0.7$ the effect is even stronger. In WBF 73.6% of the events that would be removed by this conventional cut are removed instead by the $H_1 < 0.65$ cut. For Zjj, the amount is 88.7%. We can further improve the replacement by cutting harder on H_1 so that the percentage of replacement exceeds 90% for both processes but in this case only 71.0% of events surviving all conventional cuts fulfill the FWM cut for WBF.

Considering the replacement abilities for the other cuts we see that they range between 34% and 45% for $H_1 < 0.65$ and between 75% and 83% for $H_1 < 0.2$. This means that there is a significant difference between the cutabilities for $\Delta R_{jet,jet} > 0.7$ and $y_{j_1} * y_{j_2} < 0$ and for the other cuts. So why does the cut on H_1 replace two of the other cuts so well?

First we have to think about what a cut on H_1 means in the massless case of a 2-jet event. As an example let us assume H_1 to be smaller than 0.75. Using equation (36) with $P_1(\cos\Omega) = \cos\Omega$ this translates into the requirement

$$\cos\Omega_{ij} < (0.75 \cdot (1 + 2r + r^2) - 1 - r^2)/2r = (-0.25 + 1.5r - 0.25r^2)/2r. \quad (39)$$

Within the range of 0 to 1 the right hand side of the equation becomes maximal for $r = 1$. So in this case $\cos\Omega < 0.5$. Which means that the angle between the two jets has to be at least larger than 60° The white line in Figure 16 illustrates this cut.

Cut	Cutoff[%] WBF	Replacement by single FWM acceptance cuts $H_1 < 0.75$	$H_1 < 0.65$	$H_1 < 0.2$	$H_2 > 0.5$	$H_2 > 0.9$	$H_3 < 0.65$	$H_4 > 0.75$	Combi. $H_1 < 0.65$ &$H_2 > 0.8$
cutoff in %		18.4	23.3	61.3	21.4	61.7	23.3	62.9	57.0
$\Delta R_{jet,jet} > 0.7$	3.2	68.6	73.6	98.0	6.1	47.0	63.6	49.4	85.2
$\Delta R_{jet,lep} > 0.7$	8.0	27.8	35.7	75.5	36.0	83.4	26.9	83.6	81.0
$y_{j_{min}} + 0.7 < y_{lep}$ & $y_{lep} < y_{j_{max}} - 0.7$	56.1	31.6	39.0	78.8	30.7	77.4	31.9	77.8	79.4
$y_1 * y_2 < 0$	31.0	56.4	68.5	97.5	34.2	78.8	33.8	78.5	94.5
$\lvert y_{j_1} - y_{j_2}\rvert > 4.4$	63.0	29.1	36.5	79.2	32.1	81.8	33.0	81.8	71.6
$M_{ij} > 600\,\text{GeV}$	66.4	27.4	34.3	75.5	30.4	78.8	31.3	79.5	77.6
altogether	75.1	24.4	30.8	72.0	28.2	76.4	29.7	77.1	73.1
P[%]		99.8	99.1	71.0	99.0	82.6	69.1	80.0	91.5

Table 6: Cutoff of each cut applied immediately after the initial cuts and its replacement by different cuts on FWM for WBF.

Cut	Zjj Cutoff[%]	Replacement by single FWM acceptance cuts $H_1 < 0.75$	$H_1 < 0.65$	$H_1 < 0.2$	$H_2 > 0.5$	$H_2 > 0.9$	$H_3 < 0.65$	$H_4 > 0.75$	Combi. $H_1 < 0.65$ &$H_2 > 0.8$
cutoff in %		34.4	42.3	80.4	39.7	84.6	31.9	84.8	89.5
$\Delta R_{jet,jet} > 0.7$	4.5	86.0	88.7	92.0	6.5	50.4	74.8	54.5	97.8
$\Delta R_{jet,lep} > 0.7$	14.5	28.3	36.5	77.5	43.3	89.3	27.3	89.3	88.5
$y_{j_{min}} + 0.7 < y_{lep}$ & $y_{lep} < y_{j_{max}} - 0.7$	93.8	36.4	44.5	82.5	40.4	85.3	32.7	85.4	91.4
$y_1 * y_2 < 0$	60.0	55.2	66.4	95.9	40.2	83.2	34.4	83.4	98.6
$\lvert y_{j_1} - y_{j_2} \rvert > 4.4$	95.7	36.0	44.1	82.6	40.8	85.9	32.8	85.9	91.8
$M_{ij} > 600\,\text{GeV}$	97.1	35.4	43.4	81.6	40.2	85.2	32.5	85.3	90.6
altogether	99.2	34.7	42.6	80.9	40.0	85.0	32.1	85.2	90.0
P[%]		99.9	99.4	77.7	95.0	67.3	96.9	65.5	78.2

Table 7: Cutoff of each cut applied immediately after the initial cuts and its replacement by different cuts on FWM for Zjj.

Assuming we have two massless particles that fulfill $\Delta R = 0.7$. If we further assume $\Delta y = 0$ we know that $\Delta\phi = 0.7\,\text{rad} = 40°$. If we assume instead that $\Delta\phi = 0$ we get

$$0.7 = \Delta y = \ln\left[\frac{\tan\left(\frac{\theta+\Delta\theta}{2}\right)}{\tan\left(\frac{\theta}{2}\right)}\right]. \tag{40}$$

$\Delta\theta$ becomes maximal for $\theta = 70.3°$ and $\Delta\theta = 39.3°$. These are the maximal angles that can lie between the two particles which leads us to the requirement $\Omega > 40°$ to replace the cut on 2-jet events in the massless case - which in turn is guaranteed by $H_1 < 0.75$. Actually the requirement $\Omega > 40°$ immediately translates into $H_1 < 0.88$. Of course the jets are not massless but it turns out that η and y are so close that for 2-jet events the replacement actually achieves 100% for $H_1 < 0.88$ for WBF as well as for Zjj.

For events with more than 2 hard jets, the argument remains true for the two hardest jets but a third jet can now increase H_1 so that the event is not remove. The stronger we make the cut, the less of these events which do not fulfill the ΔR condition will be kept. At the same time, the number of events removed, although they would survive the conventional cuts, decreases.

The second cut that can be replaced is $y_1 * y_2 < 0$. The explanation for this replacement is a bit more tedious. First we look at Zjj. Here we have two incoming partons which will collide. Each of the partons can emit up to two jets whereby the total number of emitted jets is reduced to two. Now we consider those events that are removed and for which two jets are detected. In general we can distinguish three cases:

Case 1. The two hardest jet can originate from one jet and it is only due to the jet clustering algorithm that they are separated. In this case it is probable that the angle between these two jets is small so that a cut on H_1 can remove this event.

Case 2. Each jet originates from each of the partons respectively. Also, the first jet has to be emitted perpendicular to the beam axis or even backwards to the propagation direction which is improbable. The second jet is emitted in the direction of propagation of the emitting parton. Now we can for example apply the cut $H_1 < 0.5$ which corresponds to the requirement $\Omega > 90°$ for 2-jet events. If the first jet is perpendicular to the beam axis, this would result in a cutoff probability of about 50% and even higher if the first jet is backward.

Case 3. Both jets arise from the same parton and are emitted into the same hemisphere. If one of the jets is forward, a cut that requires $H_1 < 0.5$ would remove nearly all events. If the rapidity of the jet approaches zero we can use the same explanation as in the second case.

For WBF the argument is quite similar. The only difference is the origin of the jets. These are generally not emitted from a parton but consist of the two partons which emit the weak boson bremsstrahlung. From the beginning these are forward backward which makes the first of the three possible cases the most likely one.

Now that we have an explanation for why the H_1 cut can replace some of the conventional cuts quite well, the question remains what happens with the other four cuts. The second ($\Delta R_{jet,lep}$) and the third cut ($y_{min} < y_l < y_{max}$) are hard to replace because they make use of the leptons. These are not considered in the FWM thus their properties can not be used. In section 5.2 we will see how far we can get without using them. Nevertheless, the conventional cuts are replaced nearly 40% of the time by the cut $H_1 < 0.65$.

The same is true for the cut on the invariant mass. There is no direct connection between the invariant mass of two jets and the angle between them, due to many other factors like their single masses and especially the absolute value of their momenta.

The cut on $\Delta y_{j_1,j_2}$ can also not be replaced explicitly. A difference in rapidity of $\Delta y = 4.4$ can correspond to a difference in $\Delta\theta$ between 56.7° and 154.7°. Thus, for a replacement we would have to ask for a minimal angle of 154.7°, but even the requirement $\Omega_{j_1,j_2} = 180°$ can not guarantee any replacement if the jets are central and the difference in angle is only caused by a difference in ϕ

The cut on H_3 shows similar characteristics as the cuts on H_1, excluding the effect of the hemisphere cut. Additionally it does not replace the conventional cuts as well as H_1 while at the same time it reduces the number of events surviving all cuts more strongly.

H_2 and H_4 do not show a preference for any conventional cut. On the contrary, they replace all cuts by the same ratio except for the first one. Instead, both cuts replace the conventional cuts better than H_1 including a higher percentage of surviving particles. Additionally, these cuts are significantly stronger on WBF than on Zjj.

In summary, we are able to replace all conventional cuts despite the first for WBF by around 80% with a cut on H_2 (or H_4). This cut reduces the signal by

17.4% but increases the signal to background ratio by a factor of 1.23. A cut on H_1, on the other hand, can especially replace the hemisphere cut and the cut on $\Delta R_{j,j}$. A good replacement combined with a high rate of surviving events can be achieved by the combination of at least two cuts as it is shown in the last column ($H_1 < 0.65 \,\&\, H_2 > 0.8$). For WBF the cuts can be replaced by 73.1% while keeping 91.5% of the events that survive the conventional cuts.

5.2 Combining Fox-Wolfram Moment Cuts

Now that we know how cuts on FWM can replace conventional cuts, we want to see what happens if we combine different cuts on Fox Wolfram moments in order to increase the signal to background ratio. The ratio that is achieved by conventional cuts is

$$r_1 = \frac{8.8\,\text{fb}}{4640\,\text{fb}} = 0.19\%. \tag{41}$$

This is the ratio we would like to achieve.

Firstly, we want to assess how a cut on one FWM influences another Fox Wolfram moment. As an example, we compare H_1 and H_2. Figure 16 shows how a cut on H_1 influences the number of events which have a certain value for H_2. We can see that a cut on H_1 doesn't result in a cut on H_2. We already know what a cut on H_1 means. Now we want to see the relation between this cut and H_2. Fig. 16 shows H_2 for 2-jet events in the r-Ω plane. The white line distinguishes between the region that is removed (underneath the line) and the one that survives. Thanks to overlapping these two graphs we see that by this cut only events with $H_2 > 0.4$ are removed.

A cut on H_1 will thus cut on another region than a cut on H_2. This means that with combinations of cuts on different FWM we may be able to make an overall cut so that the signal to background ratio will be increased.

As first try one can simply plot the FWM for both processes and normalize them to one. In the regions where the number of events is higher for the background, one makes a cut. One has to calculate the distribution again in order to see where the background again exceeds the signal. In order to compare the result with the conventional cuts, we will continue with this process until we achieve the same cross section for the background. The result of this procedure can be seen in the last line of Table 8. We can achieve a signal to background ratio of 2.41%. This is 40.8% of the signal to background ratio r_1 that is achieved by conventional cuts. This signal to background ratio uses many different cuts and is achieved by using step by step

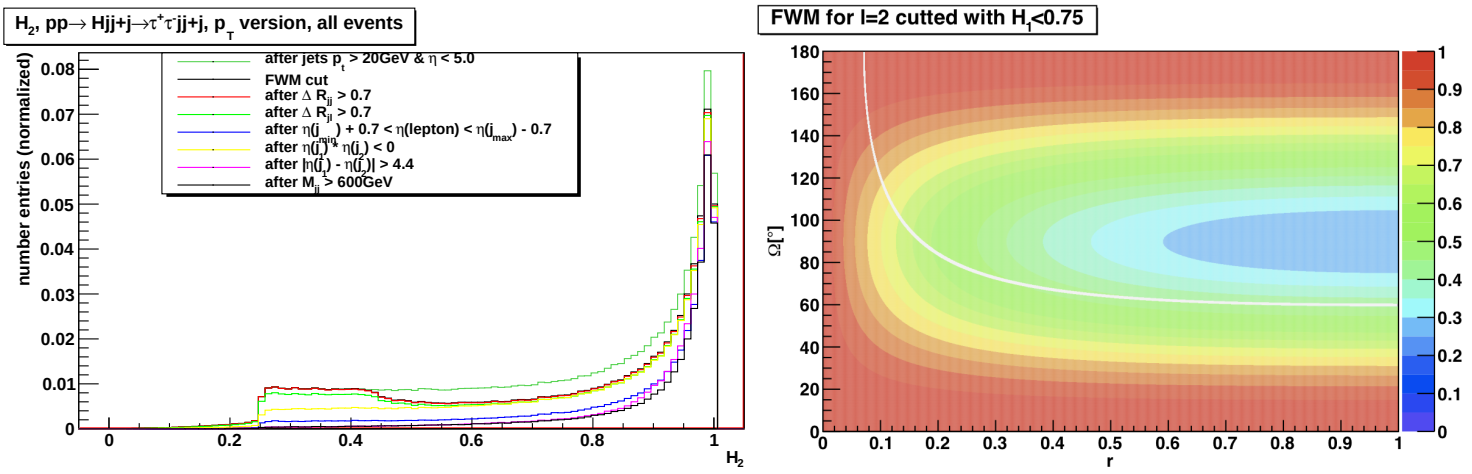

Figure 16: Influence of the acceptance cut $H_1 < 0.75$ on H_2 for all events that pass the minimal cuts

$\frac{S}{B}$	Back[fb]	Cut rep[%]		P[%]		H_1	H_2	H_3	H_4	additional cuts
		WBF	Zjj	WBF	Zjj					
5.91	37.2									conventional cuts
2.09	59.1	96.3	99.0	45.0	35.0	< 0.75	> 0.98			
2.25	46.1	97.2	99.2	38.7	29.5	< 0.75			> 0.95	
2.33	40.8	97.5	99.3	35.9	27.0	< 0.75				$H_6 > 0.91$
2.36	38.4	97.7	99.4	34.3	25.8	< 0.65				$H_8 > 0.86$
2.33	40.8	97.5	99.3	35.9	27.0	< 0.75	> 0.98			$H_6 > 0.91$
2.37	38.5	97.7	99.4	34.5	25.8	< 0.75	> 0.98			$H_8 > 0.86$
2.40	37.8	97.6	99.4	34.2	25.0	< 0.75	> 0.97			$H_{16} > 0.61$
2.41	37.7	97.7	99.4	33.7	24.6	< 0.75	> 0.97			$H_{18} > 0.56$
2.33	40.8	97.5	99.3	35.9	27.0	< 0.75			> 0.95	$H_6 > 0.91$
2.37	38.5	97.7	99.4	34.5	25.8	< 0.75			> 0.95	$H_8 > 0.86$
2.41	37.3	97.7	99.4	34.0	24.9	< 0.75			> 0.92	$H_{16} > 0.61$
2.42	37.3	97.7	99.4	33.8	24.9	< 0.75			> 0.93	$H_{18} > 0.55$
2.41	37.2	97.7	99.4	33.9	24.8	< 0.72				$H_6 > 0.87$ $H_{18} > 0.55$
2.41	37.2	97.7	99.4	34.0	25.1	< 0.7	> 0.95	< 0.7	> 0.35	$H_6 > 0.89$ $H_8 > 0.36$ $H_{16} > 0.58$ $H_{18} > 0.54$

Table 8: This table shows the signal to background ratio that is achieved by different combinations of FWM cuts. Additional informations are given by the remaining background cross section, the replacement of the cuts and the percentage P of events surviving the FWM cut in addition to the conventional cuts for both processes.

the cut that seems to be the most promising. Is this the best ratio we can achieve?

In order to investigate this, we go through all combinations of two cuts in steps of 0.01. The best results for the signal to background ratio respecting a minimal background 37.2 fb can be found in Table 8. We can achieve a signal to background ratio of 2.09 which is 35.4% of r_1 by only cutting on H_1 and H_2. By increasing the l-value of the second cut it is possible to increase the ratio by 13% to 2.36 if we cut on H_1 and H_8. The ratio can be further increased by using three instead of two cuts. The best result can be achieved by using cuts on H_1, H_4 and H_{18}. This results in a signal to background ratio of 2.42%. Thus we see that the first method already gave us a signal to background ratio near the optimum, but of course it is better to use only 3 cuts instead of 8.

Fig. 17 for example shows the FWM for $l = 7$ and $l = 14$ normalized to one after the acceptance cuts $H_1 < 0.75$, $H_4 > 0.93$ and $H_{18} > 0.55$. The FWM basically look the same for all even FWM as well as for all odd FWM. One can see that the Background process only exceeds the signal in the regions with the highest number of entries for the signal. Cutting here would dramatically decrease the signal and the background cross section. Therefore we can not use cuts on FWM to further increase the signal to background ratio without decreasing the background cross section stronger than the conventional cuts.

In the end we can state, that we can achieve a reasonably high signal to background ratio which is around 41% of the ratio achieved by conventional cuts. As the

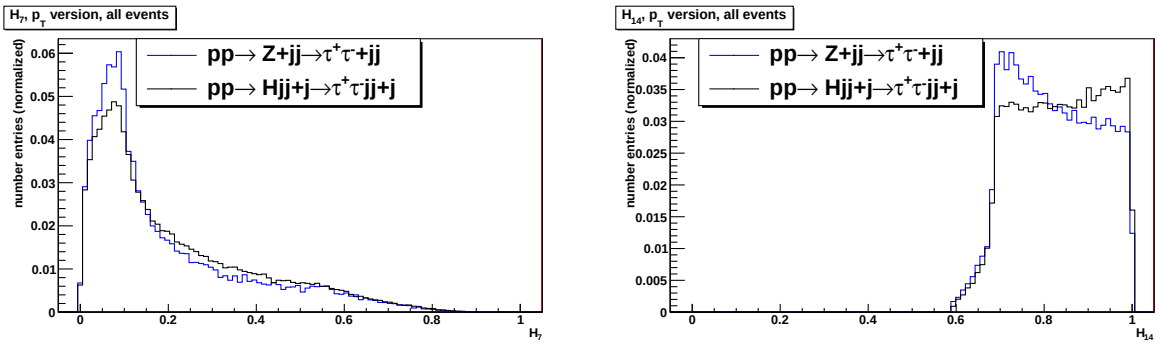

Figure 17: FWM normalized to one for both processes after the acceptance cuts $H_1 < 0.75$, $H_4 > 0.93$ and $H_{18} > 0.55$

FWM do not use the kinematical information of the leptons or the invariant mass of jets it is not surprising that we can not achieve r_1. Additionally, we could not make use of the ϕ-dependence since the jets must be forward. Possibly, FWM cuts could generate even better results for other processes that are more central. In this case a ϕ-dependence, for example due to spin interaction, would be easier to detect.

6 Conclusion

The purpose of this thesis was to investigate the possibility of using FWMs as an observable to distinguish between the signal and background processes WBF and Zjj, respectively. Using the acquired knowledge, FWM cuts can be implemented in order to replace conventional cuts. Moreover, the potential of the FWM to generate a high signal to background ratio for WBF and a background Drell-Yan process has been investigated.

At the starting point were the initial cuts, that required two leptons and two hard jets with a maximum rapidity and a minimal transverse momentum. This corresponded to a signal to background ratio of

$$r_1 = \frac{8.8\,\text{fb}}{4640\,\text{fb}} = 0.19\%. \tag{42}$$

The conventional cuts were able to increase the ratio to

$$r_2 = \frac{2.2\,\text{fb}}{37.2\,\text{fb}} = 5.9\%. \tag{43}$$

We were able to show that for WBF, cuts on H_1 and H_2 can replace the conventional cuts by 73.1% while maintaining 91.5% of the events that would not be removed by the conventional cuts. It turned out to be possible to directly replace the cut on the angular distance between two jets for 2-jet events by the acceptance cut $H_1 < 0.88$ and replace the hemisphere cut by 97.5% by requiring $H_1 < 0.2$ for WBF.

Finally, we have tried to achieve a signal to background ratio comparable to the conventional cuts by only using cuts on FWM. It was possible to achieve a ratio of

$$r_3 = \frac{0.9\,\text{fb}}{37.2\,\text{fb}} = 2.4\%. \tag{44}$$

Considering, that these cuts neither used the properties of the leptons nor the invariant mass of jets, but only geometrical properties, the result is rather good. In order to use all possible information one should further investigate the possibility of combining cuts on FWM with conventional cuts. Additionally, it would be interesting to use cuts on FWM for events that are more central. Their dependence on $\Delta\phi$ could turn out to be more useful there.

References

[1] Wikimedia Commons, `http://commons.wikimedia.org/wiki/File:Elementary_particle_interactions.svg` (September, 2 2012).

[2] bwGRiD (http://www.bw-grid.de), member of the German D-Grid initiative, funded by the Ministry for Education and Research (Bundesministerium für Bildung und Forschung) and the Ministry for Science, Research and Arts Baden-Wuerttemberg (Ministerium für Wissenschaft, Forschung und Kunst Baden-Württemberg).

[3] Wikimedia Commons, `http://commons.wikimedia.org/wiki/File:Legendrepolynomials6.svg` (September, 2 2012).

[4] Legendre polynomials. `http://en.wikipedia.org/wiki/Legendre_polynomials`. Accessed: 15/08/2012.

[5] *"OpenMP Application Program Interface, Version 3.1"*. OpenMP Architecture Review Board, July 2011.

[6] Andrea Banfi, Gavin P. Salam, and Giulia Zanderighi. "Phenomenology of event shapes at hadron colliders". *JHEP 1006 (2010) 038*.

[7] Rene Brun and Fons Rademakers. ROOT - An Object Oriented Data Analysis Framework. *Nucl. Inst. & Meth. in Phys. Res.* **A 389 (1997) 81-86.**, Proceedings AIHENP'96 Workshop, Lausanne, Sept. 1996, See also http://root.cern.ch/, 1997.

[8] M. Buschmann. "Jet Correlations in Fox-Wolfram Moments". 2012.

[9] M. Cacciari, G.P. Salam, and G. Soyez. "The anti-k_T jet clustering algorithm". *JHEP* **04 (2008) 063**, 2008.

[10] M. Cacciari, G.P. Salam, and G. Soyez. "FastJet User Manual". *EPJC* **72 (2012) 1896. arXiv:1111.6097**, Nov. 2011.

[11] F. Gianotti (ATLAS Collaboration). "Update on the Standard Model Higgs search in ATLAS". *ATLAS-CONF-2012-093*, July, 4 2012.

[12] J. Incandela (CMS Collaboration). "Update on the Standard Model Higgs search in CMS". *CMS-PAS-HIG-12-020*, July, 4 2012.

[13] M. Dobbs and J.B. Hansen. "The HepMC C++ Monte Carlo Event Record for High Energy Physics". *Comput. Phys. Commun.* **134 (2001) 41**, 2001.

[14] J. Beringer et al. (Particle Data Group). *Phys. Rev.* **D86, 010001**, 2012.

[15] R.D. Field, Y. Kanev, and M. Tayebnejad. "Topological analysis of the top quark signal and background at hadron colliders". *Phys.Rev.* **D55**, pages 5685–5697.

[16] G.C. Fox and S. Wolfram. Event Shapes in e^+e^- Annihilation. *Nucl. Phys.* **B149**, pages 413–496, 1979.

[17] L. Garren, I.G. Knowles, T. Sjöstrand, and T. Trippe. "Monte Carlo Particle Numbering Scheme". April 2002.

[18] T. Gleisberg, S. Höche, F. Krauss, M. Schönherr, S. Schumann, F. Siegert, and J. Winter. "Event generation with SHERPA 1.1". *JHEP* **02 (2009) 007**, 2009.

[19] P. W. Higgs. "Broken symmetries and the masses of gauge bosons". *Phys. Rev. Lett.***13**, 1964.

[20] P. W. Higgs. "Broken symmetries, massless particles and gauge fields". *Phys. Lett.***12**, 1964.

[21] T. Ohl and T. Darmstadt. "feynMF: Drawing Feynman Diagrams with LATEX and METAFONT". 1995.

[22] T. Plehn, D. Rainwater, and D. Zeppenfeld. "Method for identifying $H \to \tau\tau \to e^{\pm}\mu^{\mp}\not{p}_T$ at the CERN LHC". *Phys. Rev.* **D61, 093005**, 2000.

[23] S.Hoeche, S. Schuhmann, and F. Siegert. "Hard photon production and matrix element parton-showering merging". *Phys. Rev.***D81, 034026**, 2010.

Acknowledgement

First of all I have to thank Catherine Bernaciak who always had time for questions and discussions. You have been incredibly patient! Furthermore I would like to thank Tilman Plehn for always being available and making the hole project possible at all. Special thanks go to Malte Buschmann for the cooperation and to the group for cake!